nature photonics

Article

https://doi.org/10.1038/s41566-023-01331-9

Dual-chirped optical parametric amplification of high-energy single-cycle laser pulses

Received: 13 June 2023

Accepted: 13 October 2023

Published online: 19 December 2023

Check for updates

Lu Xu [1,2] & Eiji J. Takahashi [1,3]

We demonstrate how a scheme called advanced dual-chirped optical parametric amplification (DC-OPA) that employs two kinds of nonlinear crystal (BiB_3O_6 and MgO-doped lithium niobate) can generate high-energy, single-cycle mid-infrared laser pulses. In experiments, the advanced DC-OPA scheme achieved carrier-to-envelope phase-stable mid-infrared laser pulses with a bandwidth of over one octave (1.4–3.1 μm) and an output pulse energy of 53 mJ. The pulse duration was compressed to 8.58 fs, which corresponds to 1.05 cycles with a central wavelength of 2.44 μm and a peak power of 6 TW. To our knowledge, the obtained values for the pulse energy and peak power are the highest achieved for optical parametric amplification of single-cycle mid-infrared laser pulses. Moreover, owing to the energy scalability of the advanced DC-OPA scheme, the prospects of the multi-terawatt sub-cycle laser pulses are discussed.

In the past decades, breakthroughs in the generation of high-energy and few-cycle infrared (IR) or mid-infrared (MIR) lasers has improved the understanding on the interaction of intense lasers with matter, which has led to developments in a wide range of fields such as coherent X-ray high-order harmonic generation (HHG)[1], laser plasma accelerator[2], time-resolved imaging of molecular structures[3], sub-femtosecond-scale electron emission[4] and wave-packet dynamics in atoms/molecules[5]. By taking advantage of a carrier-to-envelope phase (CEP)-stable ultrafast laser pulse, the electron dynamics can be isolated in strong-field interactions, where the duration of the laser pulse is the key parameter that determines the characteristics of strong-field processes. Recently, high-energy single-cycle or even sub-cycle IR laser pulses have been drawing attention in the research field of ultrashort optics. For example, research on isolated attosecond pulse (IAP) generation via HHG phenomena requires few-cycle laser pulses. According to the 'cutoff' law of HHG, deduced with a semi-classical three-step model[6], the cutoff photon energy of a high-order harmonic spectrum extends quadratically with the wavelength of the driving laser. On the other hand, IAP emission, where the electron recombination in the HHG process is confined to a half-cycle, requires a sufficiently short pulse duration consisting of a few-cycle electric field as well as CEP stability of the driving pulse. Currently, IAP emission driven by a few-cycle IR laser source has been widely demonstrated with the output IAP energy limited to the scale of picojoules, particularly in the water-window region[7–12]. It is evident that the most direct and effective way to overcome the severe influence of HHG photon flux scaling[13] and elevate the output photon flux of IAP in the kiloelectronvolt region is to increase the pulse energy of the driving IR laser source. Given the above, to substantially scale up the photon energy, photon flux and continuum bandwidth for IAP, the development of a high-energy, single-cycle, CEP-stable laser source with a long wavelength is strongly desirable, not only in attosecond science but also in strong-field physics[2–5,14,15].

One approach to develop energetic few-cycle IR/MIR laser pulses is post-compression[16], in which high-average-power laser pulses from a conventional amplifier chain are compressed to few cycles via self-phase modulation in gases/solids[17–25]. A gas-filled antiresonant-guiding photonic crystal fibre[26] was used to achieve the least cycle number of 1.35 cycles at a central wavelength of 3.25 μm but with a pulse energy of 60 μJ. A gas-filled hollow-core fibre[27] was used to achieve the highest output pulse energy of 40 mJ, where the input pulse energy and pulse duration

[1]Ultrafast Coherent Soft X-ray Photonics Research Team, RIKEN Center for Advanced Photonics, RIKEN, Wako, Japan. [2]Attosecond Science Research Team, RIKEN Center for Advanced Photonics, RIKEN, Wako, Japan. [3]Extreme Laser Science Laboratory, RIKEN Cluster for Pioneering Research, RIKEN, Wako, Japan. e-mail: ejtak@riken.jp

https://doi.org/10.1038/s41566-023-01331-9

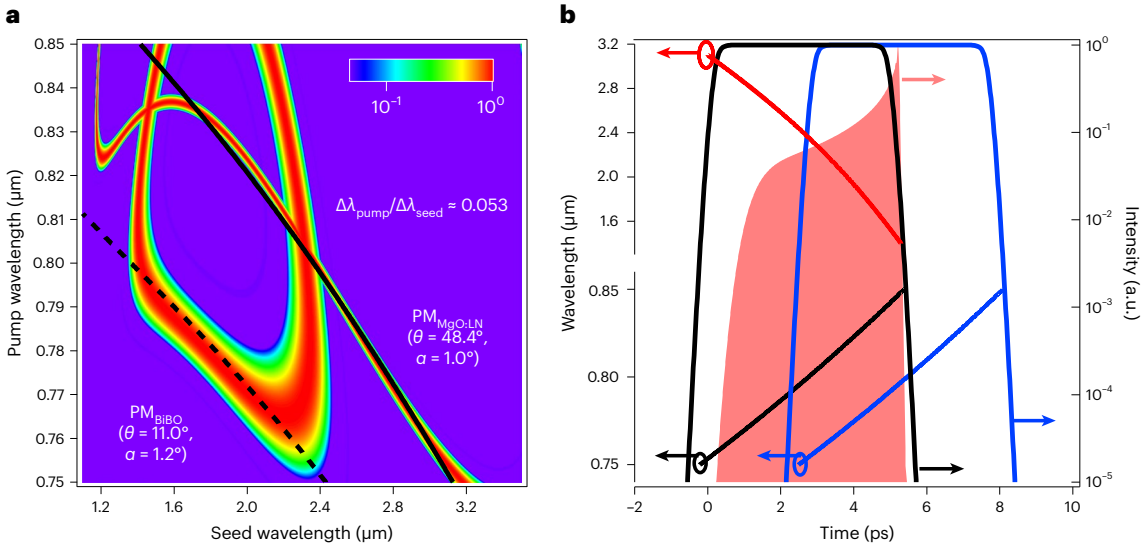

Fig. 1 | Calculated PM efficiency as a function of pump and seed laser wavelengths and the temporal overlap between the pump and seed laser pulses. a, PM efficiencies of a type-I BiBO crystal and type-I MgO:$LiNbO_3$ crystal, where the black dashed and solid lines (slopes $\Delta\lambda_{pump}/\Delta\lambda_{seed}$ of 0.053 by linear fitting) represent the wavelengths of the chirped seed laser pulse and corresponding pump laser pulse for the BiBO and MgO:$LiNbO_3$ crystals, respectively. **b**, Temporal overlap between the pump and seed laser pulses corresponding to the chirp matching in **a**. The left and right axes represent the wavelengths and normalized peak powers, respectively, corresponding to each moment in the time domain (bottom axis). The red-shaded region represents the intensity profile (right axis) of the chirped seed laser pulse in the time domain, and the red curve shows the change in wavelength (left axis) of the chirped seed laser pulse in the time domain. The black curves show the intensity profile (right axis) and change in wavelength (left axis) of the chirped pump laser pulse in the time domain to realize the chirp-matching condition in the MgO:$LiNbO_3$ crystal shown in **a**. The blue curves show the intensity profile (right axis) and change in wavelength (left axis) of the chirped pump laser in the time domain to realize the chirp-matching condition in the BiBO crystal shown in **a**.

were 70 mJ and 230 fs, respectively. However, the output temporal duration was 25 fs at 1 μm, which was not sufficient for few-cycle laser pulses. Currently, to obtain a high pulse energy with pulse duration of few-cycle (or fewer) laser pulses, the cascaded post-compression scheme was demonstrated[28], with a pulse energy of 0.98 mJ and pulse duration of 3.1 fs (1.05 cycles at 885 nm), which resulted in a peak power of 315 GW. The critical power of self-focusing was deduced[29], which was a limit to ensure that the beam does not collapse during self-phase modulation, yielding a rough estimation of power scaling with post-compression. For example, helium is commonly employed for high-energy post-compression with a gas pressure of ~1 atm. Taking the wavelength of 2 μm as an example, the critical power would be approximately 2 TW, which indicates that by using post-compression, in principle, it is difficult to achieve a peak power beyond multiple terawatts with a few-cycle pulse duration. In actual experiments, the beam quality is also a key parameter to realize the stable propagation of laser pulses via self-phase modulation. In particular, post-compression is not an amplification method for laser pulses. Therefore, it is not an ideal scheme to scale up the output energy of a single-cycle pulse.

Optical parametric amplification (OPA) is another approach that can generate/amplify a few-cycle IR/MIR laser pulse with wide frequency tunability[30–35]. A straightforward OPA scheme was employed[30] and a pulse duration of sub-two cycles centred at 1.6 μm with a pulse energy of 3 μJ was reported. However, the damage threshold of nonlinear crystals limits the energy scalability of OPA at larger pulse energies. Various schemes have been proposed to circumvent the damage to nonlinear crystals due to a high-energy pump laser, such as optical parametric chirped-pulse amplification (OPCPA)[36–40], frequency-domain OPA[41] and dual-chirped optical parametric amplification (DC-OPA)[42–47]. However, even though DC-OPA has been used to extend the pulse energy of IR/MIR laser pulses to tens or even hundreds of millijoules[47], the shortest output pulse duration is still limited to sub-two cycles because of the gain bandwidth limit of a single nonlinear crystal. Parallel waveform synthesis with OPA, which coherently combines CEP-stable laser pulses emerging from different OPA chains, has been considered as an efficient technique to realize tailored optical waveforms with sub-cycle pulse duration[48–51]. However, the pulse energy scalability is limited by the complexity of the laser system, and the highest reported output pulse energy is less than a millijoule[51]. Currently, no method has been demonstrated that can directly amplify the pulse energy of single-cycle or even sub-cycle laser pulses to multiple millijoules.

In this paper, we propose and experimentally demonstrate an amplification method called advanced DC-OPA scheme to overcome the bottleneck of pulse energy scalability in a single-cycle IR/MIR laser system. Based on the advanced DC-OPA scheme and the 10 Hz joule-class Ti:sapphire pump laser, where BiB_3O_6 (BiBO) and MgO-doped lithium niobate (MgO:$LiNbO_3$) nonlinear crystals are combined in each stage of parametric amplifiers, over-one-octave-bandwidth MIR pulses are amplified with the pulse energy of 53 mJ centred at 2.44 μm. After pulse compression using a sapphire bulk, the temporal pulse duration is down to 8.58 fs, which corresponds to 1.05 cycles at 2.44 μm. Besides that, the measured shot-to-shot stability in the single-shot CEP value is 228 mrad (root mean squared (r.m.s.)), and the evaluated M^2 values of the focused beams in the horizontal and vertical directions are 1.24 and 1.29, respectively. Finally, we discuss the possibility to demonstrate the next-generation DC-OPA, which is a high-energy, sub-cycle, CEP-stable MIR laser source, as the future prospect of the advanced DC-OPA scheme.

Advanced DC-OPA

We previously demonstrated a DC-OPA scheme using BiBO crystals with a bandwidth of 1.2–2.2 μm that achieved a pulse duration of sub-two cycles and peak power of multiple terawatts[47]. In this study, we extended the DC-OPA scheme to realize an amplified bandwidth of over one octave. However, we first need to discuss the amplified bandwidth of the DC-OPA with a single nonlinear crystal. Figure 1a plots the phase-matching (PM) efficiency (that is, $\mathrm{sinc}^2(\Delta kL/2)$) as a function of pump and seed laser wavelengths, where Δk is the phase mismatch, L is the nonlinear crystal length (set to 5 mm here) and the pump laser pulses have a fixed spectral range of 0.75–0.85 μm

https://doi.org/10.1038/s41566-023-01331-9

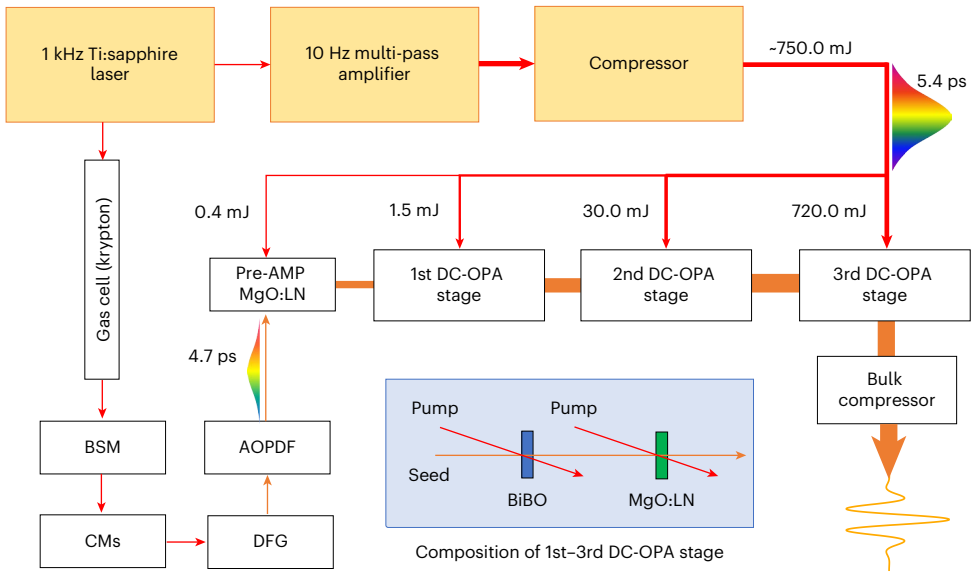

Fig. 2 | High-energy, single-cycle MIR laser source based on the advanced DC-OPA scheme. BiBO, type-I BiB_3O_6; MgO:LN, type-I MgO:$LiNbO_3$; BSM, band-stop mirror; CMs, chirped mirrors; AOPDF, acousto-optic programmable dispersive filter; DFG, difference-frequency generation. In the 1st to 3rd DC-OPA stages, the BiBO crystal is in front of the MgO:LN crystal.

corresponding to a typical chirped-pulse-amplification Ti:sapphire laser. The colour contours represent the PM efficiency relying on the combination of a type-I BiBO and type-I MgO:$LiNbO_3$ crystal (see the 'Nonlinear crystals' section). In the DC-OPA scheme, the amplified bandwidth is determined by the characteristics of the nonlinear crystals. Figure 1a indicates that MgO:$LiNbO_3$ may be able to realize an amplified bandwidth of one octave (1.6–3.2 μm) under the linear chirped configuration. However, this ideal case is not easy to realize because the chirp configuration of the seed laser pulse in the experimental setup cannot be as linear as that of the pump laser pulse. In the advanced DC-OPA scheme, we smoothly connect the PM regions (Fig. 1a, colour contours) and optimize the chirp matching (see the 'Chirp matching' section) between the pump and seed laser pulses to achieve an amplified bandwidth of over one octave by the combination of two kinds of nonlinear crystal in parametric amplification. Considering the transmittance and gain bandwidth of commonly used nonlinear crystals, the BiBO and MgO:$LiNbO_3$ crystals have been finally chosen as the nonlinear medium for the amplification of an MIR laser source based on the advanced DC-OPA scheme.

Experimental setup

Figure 2 illustrates the experimental setup of a high-energy, single-cycle CEP-stable MIR laser system based on the proposed advanced DC-OPA scheme. Compared with the previously reported system[47], we made several major upgrades to obtain high-energy single-cycle MIR laser pulses. Specifically, (1) the Ti:sapphire pulses with a total pulse energy of 750 mJ and pulse duration of ~5.7 ps (full width at 10^{-3}, nearly linear negative chirp) were applied as the pump for the advanced DC-OPA. (2) The passively CEP-stable, over-one-octave MIR (1.4–3.1 μm) seed laser pulses were generated via difference-frequency generation (DFG) in a type-II BiBO crystal (see the 'Nonlinear crystals' section), whose spectrum is shown in Fig. 3 (black-filled profile). After stretching in the acousto-optic programmable dispersive filter (AOPDF; DAZZLER/HR45-1450-3000), the MIR seed laser pulses, with a dispersion predominantly given as the inverse of the sapphire bulk compressor and pulse duration of ~4.7 ps (full width at 10^{-3}), were produced as the seed for the advanced DC-OPA. (3) There was one pre-amplification stage using the MgO:$LiNbO_3$ crystal and three amplification stages combining two kinds of nonlinear

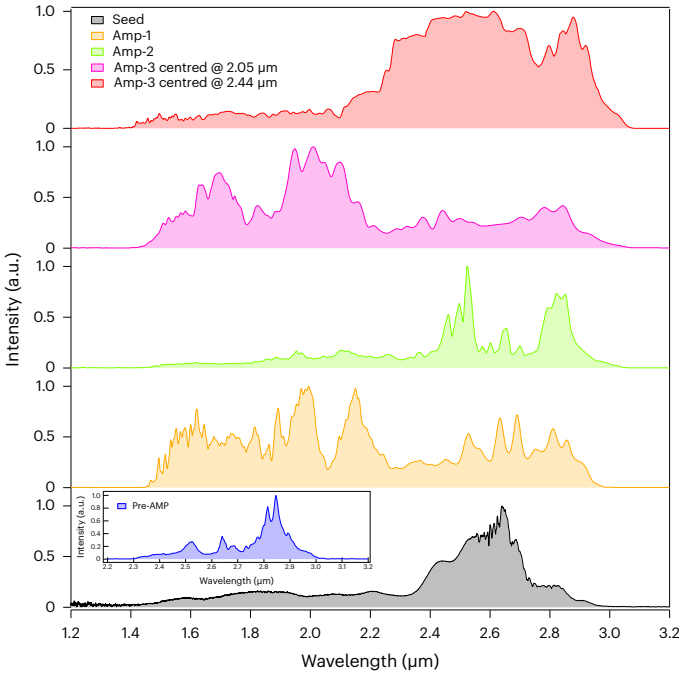

Fig. 3 | Evolution of the laser spectrum. Input seed spectrum for advanced DC-OPA (black solid line with filling), output of the pre-amplifier based on MgO:$LiNbO_3$ (blue solid line with filling), output of the first amplifier based on BiBO and MgO:$LiNbO_3$ (orange solid line with filling), output of the second amplifier based on BiBO and MgO:$LiNbO_3$ (green solid line with filling) and output of the third amplifier based on BiBO and MgO:$LiNbO_3$ (pink solid line with filling and red solid line with filling for the central wavelength of 2.05 and 2.44 μm, respectively).

crystal (that is, BiBO and MgO:$LiNbO_3$) in the advanced DC-OPA (see the 'Nonlinear crystals' section). We employed the pre-amplification stage to compensate for absorption by the BiBO crystals in the subsequent amplifiers of wavelengths longer than 2.4 μm and the difference in quantum efficiency of different wavelengths during the parametric amplification process. In contrast to the pre-amplifier, each of the three subsequent amplifiers contained a BiBO crystal

https://doi.org/10.1038/s41566-023-01331-9

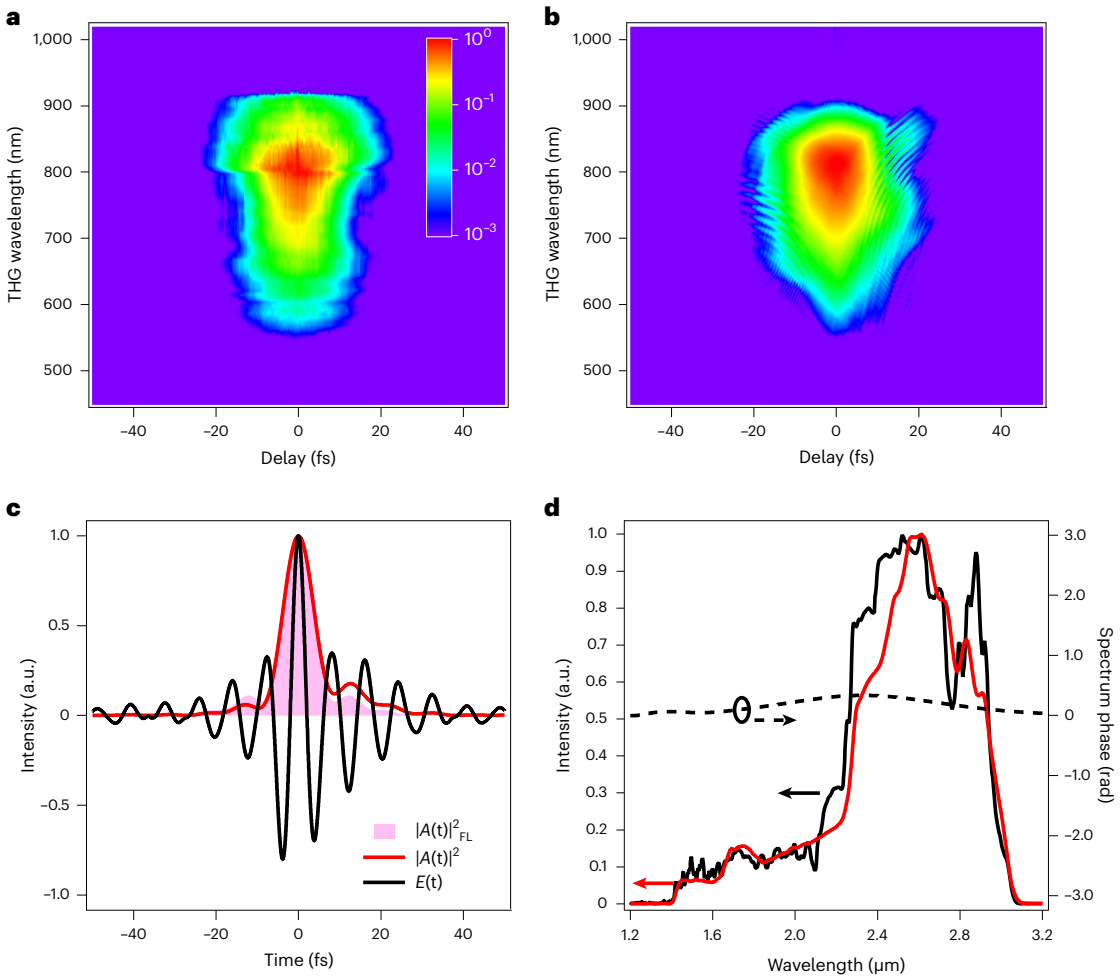

Fig. 4 | THG-FROG results of the MIR laser pulses based on the advanced DC-OPA scheme. a, Measured THG-FROG traces with a central wavelength of 2.44 μm. **b**, Retrieved THG-FROG traces corresponding to the data in **a** with an error of 0.78%. **c**, Reconstructed temporal profile with a pulse duration of 8.58 fs (full-width at half-maximum), where the electric-field profile (black solid line) under the cosine-like waveform (carrier wavelength, 2.44 μm) and its squared envelope (red solid line; TL shown in pink filling) are shown, respectively. **d**, Reconstructed spectrum (red solid line) and spectral phase (black dash line), and the measured spectrum of the final output centred at 2.44 μm (black solid line).

and a MgO:$LiNbO_3$ crystal, and the BiBO crystal was in front of the MgO:$LiNbO_3$ crystal to reduce the effect of absorption by BiBO on the final output pulse energy. (4) The focusing geometry is employed for the interacting laser pulses in both pre-amplifier and first-stage amplifier. The nonlinear crystals were placed in the overlap of the Rayleigh lengths for the pump and seed beams to maintain a good PM condition between the pump and seed lasers. In the second and third amplifiers, both pump and seed laser pulses were collimated. Supplementary Table 1 lists the parameters used in each amplification stage and the output performance of each amplifier.

Experimental results

By adjusting the non-collinear angle and time delay between the pump and seed introduced in each nonlinear crystal, the combination of the pre-amplifier (MgO:$LiNbO_3$) and first amplifier (BiBO and MgO:$LiNbO_3$) realized a relatively balanced amplification of the full spectrum at 1.4–3.1 μm (Fig. 3, orange-filled profile). In the second amplifier stage, the MgO:$LiNbO_3$ crystal was thicker than the BiBO crystal and was subjected to a higher pump power intensity, so the central wavelength of the amplified spectrum after the second stage was shifted towards the longer-wavelength band (Fig. 3, green-filled profile). It is worth noting that a higher pump power intensity was applied to the MgO:$LiNbO_3$ crystal than that to the BiBO crystal in the last amplifier (Supplementary Table 1, 3rd stage_2); the MIR laser system obtained a final output pulse energy of 53 mJ with a total conversion efficiency from the pump laser to seed laser of 7%. To consider the number of cycles in a pulse envelope, we applied the centre-of-gravity concept, which has been recognized to determine the carrier wavelength (that is, the central wavelength) of laser pulses[50], to define the central wavelength of the spectrum. According to this concept, the central wavelength of the output spectrum (Fig. 3, red-filled profile) after the final amplifier stage was 2.44 μm. Owing to these optimizations, an over-one-octave (1.4–3.1 μm) output bandwidth with a pulse energy of >50 mJ was attained based on the advanced DC-OPA scheme.

Moreover, when the pump laser energies allocated to the two crystals in the last amplifier were exchanged, that is, a higher pump laser energy was applied to the BiBO crystal (Supplementary Table 1, 3rd stage_1), the amplification energy of the final stage was increased to 61 mJ, but the central wavelength shifted to 2.05 μm (Fig. 3, pink-filled profile), which was because a higher gain was achieved in the short-wavelength region than in the long-wavelength region with this pump arrangement. This demonstrated another advantage of the advanced DC-OPA scheme: the tunability of the central wavelength.

After the amplification, a 40-mm-long sapphire bulk compressor was employed to temporally compress the MIR laser pulses with the diameter of the beam expanded to 60 mm (the calculated *B*-integral was 0.11). To characterize the temporal duration of the compressed pulses with an over-one-octave bandwidth, third-order harmonic generation frequency-resolved optical gating (THG-FROG) was adopted

https://doi.org/10.1038/s41566-023-01331-9

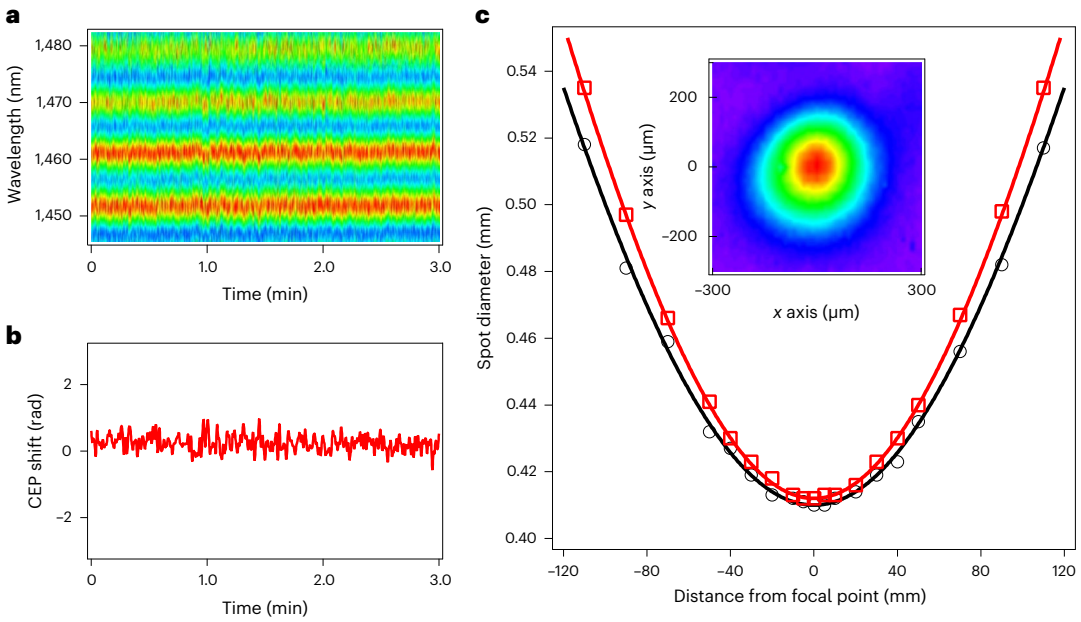

Fig. 5 | Measurements of the single-shot CEP in the *f*-to-2*f* interferometer and beam quality. a, Temporal evolution of the *f*-to-2*f* spectral interference fringes, where a single shot of the spectrum was obtained for each record. **b**, CEP shift extracted from the spectrogram depicted in **a**. The r.m.s. error of the CEP shift was evaluated to be 228 mrad. **c**, Evolution of the beam diameters (full width at e^{-2} maximum) along the *x* axis (horizontal direction, black circles) and *y* axis (vertical direction, red squares) with the beam propagation across the focal point. The evaluated M^2 values for the *x* and *y* axes by fitting each measured diameter were 1.24 (black solid line) and 1.29 (red solid line), respectively. The corresponding beam profile at the focal point is shown in the inset.

for the MIR laser pulses (see the 'Pulse duration' section). To fully compress the MIR laser pulses, the dispersion loaded in the AOPDF should be strictly optimized. Thus, the spectral phases of the measured laser pulses, which were retrieved from the THG-FROG traces, were fed back to the AOPDF for the modification of dispersion compensation. After several iterations to correct the preset spectral phase in the AOPDF, the fully compressed MIR laser pulses with a central wavelength of 2.44 μm were obtained with a nearly flat spectral phase (Fig. 4). The spectral intensity and spectral phase, which were retrieved from the measured THG-FROG traces (Fig. 4a), were demonstrated by the red solid line and black dashed line, respectively (Fig. 4d). The coincidence of the reconstructed spectrum (red solid line) and measured spectrum (black solid line) in terms of the range and trend of the wavelengths (Fig. 4d) further proved that complete compression with a full bandwidth was achieved. The corresponding temporal pulse profiles of the retrieved pulses with a pulse duration of 8.58 fs (full-width at half-maximum) and transform-limited (TL) pulse duration of 8.22 fs are illustrated in Fig. 4c, which correspond to a 1.05-cycle duration of the electric field at a central wavelength of 2.44 μm and result in a peak power of 6 TW. In addition, the output MIR laser pulses with a pulse energy of 61 mJ and central wavelength of 2.05 μm were also measured via THG-FROG, in which the temporal pulse profiles with a pulse duration of 8.75 fs and a TL pulse duration of 8.18 fs were achieved. This indicated that the MIR laser pulses had a pulse duration of 1.28 cycles and peak power of 7 TW.

Subsequently, a home-built single-shot *f*-to-2*f* interferometer was implemented after the sapphire bulk compressor to characterize the CEP stability of the MIR laser pulse. The time evolution of the *f*-to-2*f* interference fringes, which were in the wavelength region of 1.45–1.48 μm, is shown in Fig. 5a. The CEP values extracted from the spectrogram (Fig. 5a), which included 1,800 consecutive records with single-shot CEP, are demonstrated in Fig. 5b with an r.m.s. value of 228 mrad for 3 min.

Meanwhile, the quality of the focus beam profile is one of the great concerns in the strong-field experiments. The measured beam profile with a diameter of ~410 μm (full width at e^{-2}) on the focus plane is shown in Fig. 5c (inset). Concurrently, the diameter evolutions of the focusing beam profile up to two times the Rayleigh length across the focal point are recorded in the horizontal (Fig. 5c, black circles) and vertical (Fig. 5c, red squares) directions, respectively. The obtained M^2 values (defined at the central wavelength of 2.44 μm) of the focus beam profile were 1.24 and 1.29 in the horizontal and vertical directions, respectively.

Prospects and conclusion

Owing to the various types and numbers of nonlinear crystal combined in the advanced DC-OPA scheme, one of the obvious advantages is its excellent energy scalability. Specifically, (1) in this paper, since the Ti:sapphire laser was used as the pump of the advanced DC-OPA scheme, the optimal combination scheme of BiBO and MgO:$LiNbO_3$ crystals was finally adopted. For pump lasers with other wavelength regions, similar crystal combination methods (crystal types are not limited to BiBO and MgO:$LiNbO_3$) can be used to achieve ultrabroadband parametric amplification. (2) In this study, we used a two-crystal combination mode, which was mainly limited by the bandwidth of the AOPDF and total pump laser energy in the experiment. In particular, based on a wider-bandwidth dispersion control device and higher total pump energy, a combination of multiple crystals can be used to achieve a broader-bandwidth parametric amplification and obtain a sub-cycle pulse duration. As future prospects, we discuss the advanced DC-OPA scheme to amplify the sub-cycle MIR laser pulses based on the experimental results of a single-cycle pulse, where the longest wavelength of the amplified MIR laser has reached the limitation of transmission in BiBO as 3.4 μm.

Regarding the PM efficiency (Fig. 6a), the seed laser pulses within the wavelength range of 1.2–3.4 μm can be successfully amplified based on the advanced DC-OPA scheme. To maintain amplification with a broad bandwidth of nearly two octaves, the dispersion management of the pump and seed laser pulses is extremely critical. Chirp matching (Methods) indicates that the MIR laser pulses with a bandwidth of 1.8 octaves are fully amplified by the advanced DC-OPA scheme. Compared with the single-cycle experiments, the designed amplifier has the following differences. (1) Two MgO:$LiNbO_3$ crystals are used in the pre-amplification stage to compensate for the difference in subsequent absorption loss and quantum efficiency. (2) There are three crystals (Bi

https://doi.org/10.1038/s41566-023-01331-9

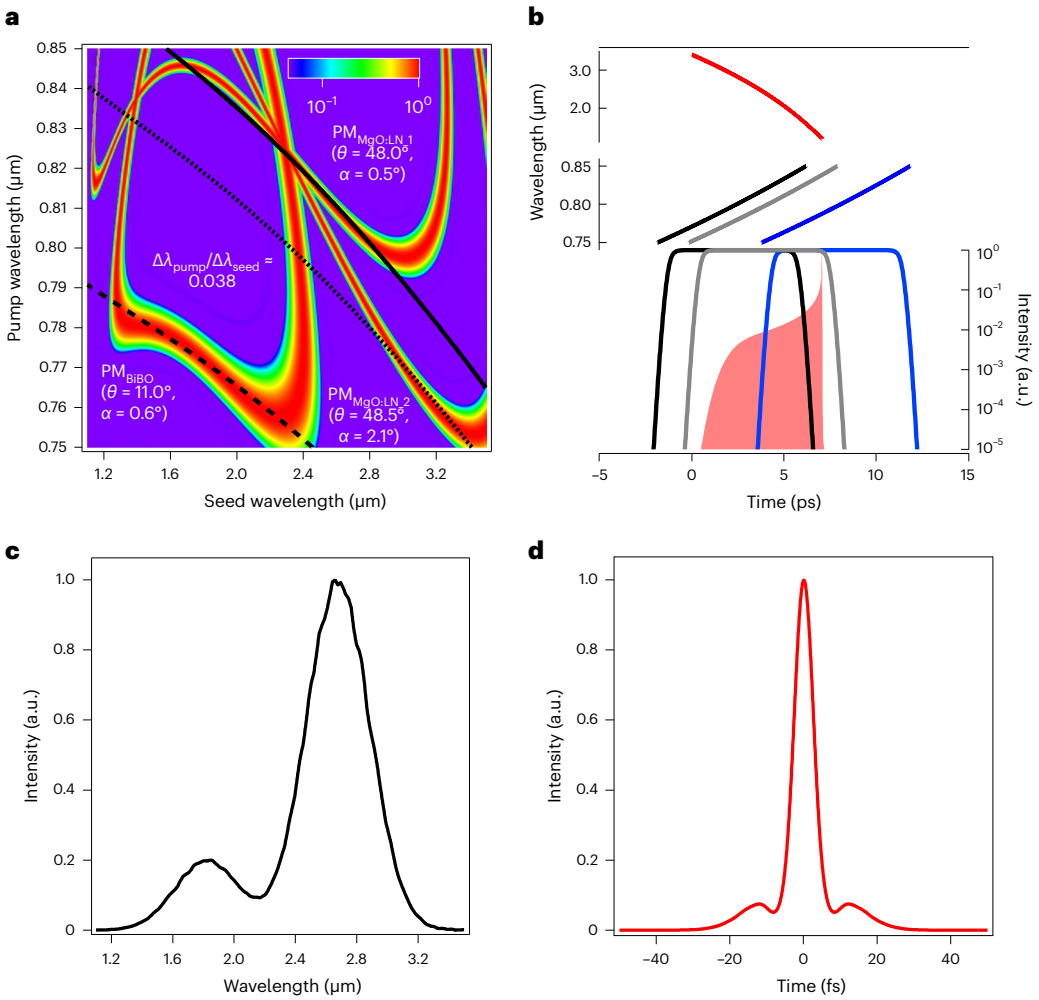

Fig. 6 | Calculated PM efficiency as a function of pump and seed laser wavelengths, the temporal overlap between the pump and seed laser pulses, simulated final output spectrum and corresponding TL pulse duration. a, PM efficiency combining type-I BiBO and type-I MgO:$LiNbO_3$ crystals. The black dashed, solid and dotted lines (slopes ($\Delta\lambda_{pump}/\Delta\lambda_{seed}$) of 0.038 by linear fitting) represent the wavelengths of the chirped seed laser pulse and the corresponding pump laser pulse for the BiBO and MgO:$LiNbO_3$ crystals, respectively. **b**, Temporal overlap between the pump and seed laser pulses corresponding to the chirp matching in **a**. The left and right axes represent the wavelengths and normalized peak powers, respectively, corresponding to each moment in the time domain (bottom axis). The red-shaded region represents the intensity profile (right axis) of the chirped seed laser pulse in the time domain, and the red curve shows the change in wavelength (left axis) of the chirped seed laser pulse in the time domain. The black curves show the intensity profile (right axis) and change in wavelength (left axis) of the chirped pump laser pulse in the time domain to realize the chirp-matching condition in the first MgO:$LiNbO_3$ crystal shown in **a**. The grey curves show the intensity profile (right axis) and change in wavelength (left axis) of the chirped pump laser pulse in the time domain to realize the chirp-matching condition in the second MgO:$LiNbO_3$ crystal shown in **a**. The blue curves show the intensity profile (right axis) and change in wavelength (left axis) of the chirped pump laser pulse in the time domain to realize the chirp-matching condition in the BiBO crystal shown in **a**. **c**, Simulated final output spectrum of the designed sub-cycle MIR laser system. **d**, Corresponding TL pulse duration of the spectrum shown in **c**.

BO + MgO:$LiNbO_3$ + MgO:$LiNbO_3$) in each amplification stage to ensure an effective amplification of the full bandwidth. Based on the numerical simulation model[46] and Ti:sapphire pump laser pulses with a total pulse energy of over 1 J, the calculated final output spectrum and corresponding TL pulse duration are shown in Fig. 6c,d, respectively. The simulated output pulse energy reached 65 mJ with a total conversion efficiency of approximately 6.5%. This indicated that the MIR laser pulses with a bandwidth of 1.8 octaves were fully amplified by the advanced DC-OPA scheme, which supported the TL pulse duration (6.2 fs) of 0.75 cycles at 2.47 μm. In addition, the advanced DC-OPA scheme can be expanded in the case of Yb laser pumping. The current Yb thin-disc technology can provide a few hundreds of watts of average power. By broadening the bandwidth of the Yb laser via nonlinear interactions[52], the Yb laser can be employed as a pump laser for the advanced DC-OPA. As a result, an over 10 mJ MIR single-cycle pulse with an over kilohertz repetition rate will be realized by combining Yb lasers at hundreds of watts and proper nonlinear crystals. The advanced DC-OPA scheme for amplifying the single-cycle pulse will break not only the pulse energy bottleneck but also the average power bottleneck.

To our knowledge, this is the first time that an amplification method has been demonstrated for single-cycle laser pulses. Based on the optimized experimental setup of the advanced DC-OPA scheme, where the combination of type-I BiBO and type-I MgO:$LiNbO_3$ nonlinear crystals was employed in the parametric amplification, an over 50 mJ, single-cycle (8.58 fs at 2.44 μm), 10 Hz, CEP-stable (228 mrad (r.m.s.)) MIR laser source was demonstrated, resulting in a peak power of 6 TW. Furthermore, the prospect of a high-energy MIR laser source towards sub-cycle pulse duration was discussed by extending the combination of nonlinear crystals in the advanced DC-OPA scheme. In strong-field physics dealing with the interaction of laser with matter, the 'cycle number of the electric field' within a pulse envelope plays an extremely important role. Especially, the cycle number strongly affects

the continuous range of HHG spectrum. When the cycle numbers of the driving laser pulses are 2.0, 1.0 and 0.7 within a Gaussian envelope, the corresponding percentages of the continuum region in the HHG spectrum are approximately 15%, 50% and 73%, respectively—that is, the continuum bandwidth reaches 500 eV at the 1-keV-cutoff photon energy pumped by a single-cycle laser pulse. The fewer-cycles MIR laser source based on the advanced DC-OPA scheme present the potential for the generation of X-rays with a duration of several attoseconds (even zeptoseconds), which would offer a breakthrough progress in the electron dynamics and correlations. Moreover, owing to the excellent energy scalability of this advanced DC-OPA scheme, it is reasonable to obtain laser pulses with higher pulse energy and fewer cycle numbers of pulse duration based on different crystal combinations and a higher pump energy. The expansion of pulse energy can facilitate high-flux detection conditions for research in strong-field physics. Meanwhile, sub-cycle (even half-cycle) laser pulses can effectively avoid the superposition of phenomena caused by periodic oscillations of the laser field in the laser–matter interaction under strong-field conditions, which can make the research results more intuitive and accurate.

Online content

Any methods, additional references, Nature Portfolio reporting summaries, source data, extended data, supplementary information, acknowledgements, peer review information; details of author contributions and competing interests; and statements of data and code availability are available at https://doi.org/10.1038/s41566-023-01331-9.

References

1. Krausz, F. & Ivanov, M. Attosecond physics. *Rev. Mod. Phys.* **81**, 163 (2009).
2. Esarey, E., Schroeder, C. B. & Leemans, W. P. Physics of laser-driven plasma-based electron accelerators. *Rev. Mod. Phys.* **81**, 1229 (2009).
3. Blaga, C. I. et al. Imaging ultrafast molecular dynamics with laser-induced electron diffraction. *Nature* **483**, 194–197 (2012).
4. Herink, G., Solli, D. R., Gulde, M. & Ropers, C. Field-driven photo emission from nanostructures quenches the quiver motion. *Nature* **483**, 190–193 (2012).
5. Goulielmakis, E. et al. Real-time observation of valence electron motion. *Nature* **466**, 739–743 (2010).
6. Corkum, P. B. Plasma perspective on strong field multiphoton ionization. *Phys. Rev. Lett.* **71**, 1994 (1993).
7. Herrero, C. et al. Generation of broad XUV continuous high harmonic spectra and isolated attosecond pulses with intense mid-infrared lasers. *J. Phys. B: At. Mol. Opt. Phys.* **45**, 011001 (2012).
8. Ishii, N. et al. Carrier-envelope phase-dependent high harmonic generation in the water window using few-cycle infrared pulses. *Nat. Commun.* **5**, 3331 (2014).
9. Silva, F., Teichmann, S. M., Cousin, S. L., Hemmer, M. & Biegert, J. Spatiotemporal isolation of attosecond soft X-ray pulses in the water window. *Nat. Commun.* **6**, 6611 (2015).
10. Teichmann, S. M., Silva, F., Cousin, S. L., Hemmer, M. & Biegert, J. 0.5-keV soft X-ray attosecond continua. *Nat. Commun.* **7**, 11493 (2016).
11. Li, J. et al. 53-attosecond X-ray pulses reach the carbon K-edge. *Nat. Commun.* **8**, 186 (2017).
12. Schmidt, C. et al. High-order harmonic source spanning up to the oxygen K-edge based on filamentation pulse compression. *Opt. Express* **26**, 11834–11842 (2018).
13. Tate, J. et al. Scaling of wave-packet dynamics in an intense midinfrared field. *Phys. Rev. Lett.* **98**, 013901 (2007).
14. Milošević, D. B., Paulus, G. G., Bauer, D. & Becker, W. Above-threshold ionization by few-cycle pulses. *J. Phys. B: At. Mol. Opt. Phys.* **39**, R203 (2006).
15. Nubbemeyer, T., Gorling, K., Saenz, A., Eichmann, U. & Sandner, W. Strong-field tunneling without ionization. *Phys. Rev. Lett.* **101**, 233001 (2008).
16. Duguay, M. & Hansen, J. Compression of pulses from a mode-locked He–Ne laser. *Appl. Phys. Lett.* **14**, 14–16 (1969).
17. Mücke, O. D. et al. Self-compression of millijoule 1.5 μm pulses. *Opt. Lett.* **34**, 2498–2500 (2009).
18. Cardin, V. et al. 0.42 TW 2-cycle pulses at 1.8 μm via hollow-core fiber compression. *Appl. Phys. Lett.* **107**, 181101 (2015).
19. Zou, X. et al. 300 μJ, 3 W, few-cycle, 3 μm OPCPA based on periodically poled stoichiometric lithium tantalate crystals. *Opt. Lett.* **44**, 2791–2794 (2019).
20. Kurucz, M. et al. 2.3-cycle mid-infrared pulses from hybrid thin-plate post-compression at 7 W average power. *Opt. Commun.* **472**, 126035 (2020).
21. Hemmer, M., Baudisch, M., Thai, A., Couairon, A. & Biegert, J. Self-compression to sub-3-cycle duration of mid-infrared optical pulses in dielectrics. *Opt. Express* **21**, 28095–28102 (2013).
22. Sanari, Y. et al. Generation of wavelength-tunable few-cycle pulses in the mid-infrared at repetition rates up to 10 kHz. *Opt. Lett.* **46**, 5280–5283 (2021).
23. Fan, G. et al. Hollow-core-waveguide compression of multi-millijoule CEP-stable 3.2 μm pulses. *Optica* **3**, 1308–1311 (2016).
24. Lu, F. et al. Generation of sub-two-cycle CEP-stable optical pulses at 3.5 μm from a KTA-based optical parametric amplifier with multiple-plate compression. *Opt. Lett.* **43**, 2720–2723 (2018).
25. Li, C. et al. Generation of carrier-envelope phase stabilized intense 1.5 cycle pulses at 1.75 μm. *Opt. Express* **19**, 6783–6789 (2011).
26. Elu, U. et al. High average power and single-cycle pulses from a mid-IR optical parametric chirped pulse amplifier. *Optica* **4**, 1024–1029 (2017).
27. Fan, G. et al. 70 mJ nonlinear compression and scaling route for an Yb amplifier using large-core hollow fibers. *Opt. Lett.* **46**, 896–899 (2021).
28. Tsai, M. S. et al. Nonlinear compression toward high-energy single-cycle pulses by cascaded focus and compression. *Sci. Adv.* **8**, eabo1945 (2022).
29. Fibich, G. & Gaeta, A. L. Critical power for self-focusing in bulk media and in hollow waveguides. *Opt. Lett.* **25**, 335–337 (2000).
30. Brida, D. et al. Sub-two-cycle light pulses at 1.6 μm from an optical parametric amplifier. *Opt. Lett.* **33**, 741–743 (2008).
31. Takahashi, E. J., Kanai, T., Nabekawa, Y. & Midorikawa, K. 10 mJ class femtosecond optical parametric amplifier for generating soft X-ray harmonics. *Appl. Phys. Lett.* **93**, 041111 (2008).
32. Andriukaitis, G. et al. 90 GW peak power few-cycle mid-infrared pulses from an optical parametric amplifier. *Opt. Lett.* **36**, 2755–2757 (2011).
33. Thiré, N. et al. 10 mJ 5-cycle pulses at 1.8 μm through optical parametric amplification. *Appl. Phys. Lett.* **106**, 091110 (2015).
34. Kanai, T. et al. Parametric amplification of 100 fs mid-infrared pulses in $ZnGeP_2$ driven by a Ho:YAG chirped-pulse amplifier. *Opt. Lett.* **42**, 683–686 (2017).
35. Chen, B. H., Wittmann, E., Morimoto, Y., Baum, P. & Riedle, E. Octave-spanning single-cycle middle-infrared generation through optical parametric amplification in $LiGaS_2$. *Opt. Express* **27**, 21306–21318 (2019).
36. Ishii, N. et al. Sub-two-cycle, carrier-envelope phase-stable, intense optical pulses at 1.6 μm from a BiB_3O_6 optical parametric chirped-pulse amplifier. *Opt. Lett.* **37**, 4182–4184 (2012).
37. Yin, Y. et al. High-efficiency optical parametric chirped-pulse amplifier in BiB_3O_6 for generation of 3 mJ, two-cycle, carrier-envelope-phase-stable pulses at 1.7 μm. *Opt. Lett.* **41**, 1142–1145 (2016).

38. Bigler, N. et al. High-power OPCPA generating 1.7 cycle pulses at 2.5 µm. *Opt. Express* **26**, 26750–26757 (2018).
39. Zhou, F., Wu, Y., Marra, A. & Chang, Z. Efficient generation of femtosecond millijoule pulses at 3.1 µm. *Opt. Lett.* **47**, 6057–6060 (2022).
40. Grafenstein, L. V. et al. Multi-millijoule, few-cycle 5 µm OPCPA at 1 kHz repetition rate. *Opt. Lett.* **45**, 5998–6001 (2020).
41. Schmidt, B. E. et al. Frequency domain optical parametric amplification. *Nat. Commun.* **5**, 3643 (2014).
42. Zhang, Q., Takahashi, E. J., Mücke, O. D., Lu, P. & Midorikawa, K. Dual-chirped optical parametric amplification for generating few hundred mJ infrared pulses. *Opt. Express* **19**, 7190–7212 (2011).
43. Fu, Y., Takahashi, E. J. & Midorikawa, K. High-energy infrared femtosecond pulses generated by dual-chirped optical parametric amplification. *Opt. Lett.* **40**, 5082–5085 (2015).
44. Fu, Y., Xue, B., Midorikawa, K. & Takahashi, E. J. TW-scale mid infrared pulses near 3.3 µm directly generated by dual-chirped optical parametric amplification. *Appl. Phys. Lett.* **112**, 241105 (2018).
45. Fu, Y., Midorikawa, K. & Takahashi, E. J. Towards a petawatt-class few-cycle infrared laser system via dual-chirped optical parametric amplification. *Sci. Rep.* **8**, 7692 (2018).
46. Xu, L. et al. Optimization of a multi-TW few-cycle 1.7-µm source based on type-I BBO dual-chirped optical parametric amplification. *Opt. Express* **28**, 15138–15147 (2020).
47. Xu, L. et al. 100-mJ class, sub-two-cycle, carrier-envelope phase-stable dual-chirped optical parametric amplification. *Opt. Lett.* **47**, 3371–3374 (2022).
48. Huang, S. et al. High-energy pulse synthesis with sub-cycle waveform control for strong-field physics. *Nat. Photon* **5**, 475–479 (2011).
49. Liang, H. et al. High-energy mid-infrared sub-cycle pulse synthesis from a parametric amplifier. *Nat. Commun.* **8**, 141 (2017).
50. Lin, Y., Nabekawa, Y. & Midorikawa, K. Optical parametric amplification of sub-cycle shortwave infrared pulses. *Nat. Commun.* **11**, 3413 (2020).
51. Rossi, G. M. et al. Sub-cycle millijoule-level parametric waveform synthesizer for attosecond science. *Nat. Photon.* **14**, 629–635 (2020).
52. Pfaff, Y. et al. Nonlinear pulse compression of a 200 mJ and 1 kW ultrafast thin-disk amplifier. *Opt. Express* **31**, 22740–22756 (2023).

Publisher's note Springer Nature remains neutral with regard to jurisdictional claims in published maps and institutional affiliations.

Open Access This article is licensed under a Creative Commons Attribution 4.0 International License, which permits use, sharing, adaptation, distribution and reproduction in any medium or format, as long as you give appropriate credit to the original author(s) and the source, provide a link to the Creative Commons license, and indicate if changes were made. The images or other third party material in this article are included in the article's Creative Commons license, unless indicated otherwise in a credit line to the material. If material is not included in the article's Creative Commons license and your intended use is not permitted by statutory regulation or exceeds the permitted use, you will need to obtain permission directly from the copyright holder. To view a copy of this license, visit http://creativecommons.org/licenses/by/4.0/.

© The Author(s) 2023

Methods

Chirp matching

To achieve amplification with a broad bandwidth in the advanced DC-OPA scheme, the most critical aspect is the chirp management of pump and seed laser pulses. Specifically, pump laser pulses, which are stretched using grating pairs, have an almost-linear chirp. Meanwhile, seed laser pulses, which are stretched in the AOPDF and then compressed in the bulk material, have a nonlinear chirp. Under the PM condition, the one-to-one correspondence between the seed and pump laser wavelengths in the form of curves is evident (Fig. 1a, dashed and solid black lines). These curves are linearly fitted to a slope ($\Delta\lambda_{pump}/\Delta\lambda_{seed}$) of 0.053 to intuitively show the chirp-matching relationship between the pump and seed laser pulses. To fully utilize the pump energy and prevent damage to the nonlinear crystal, the laser pulses in the DC-OPA amplifiers need to be stretched to the order of several picoseconds in advance. Therefore, we employed sapphire bulk with a length of 40 mm as a compressor to achieve a compression of several picoseconds. As shown in Fig. 1a, the dashed black line exhibits that the chirp matching between the seed laser pulse (bottom axis) and corresponding pump laser pulse (left axis) is well within the PM region of the BiBO crystal, which indicates broadband parametric amplification with a wavelength of 1.4–2.4 μm. When the same chirp-matching relationship is shifted to the PM region of the MgO:$LiNbO_3$ crystal (Fig. 1a, solid black line), it shows that the overlapping part can support parametric amplification with a wavelength of 2.2–3.1 μm. For chirped pulses, chirp matching is reflected not only by the correspondence of wavelengths in the frequency domain but also by the overlapping positions of the pump and seed laser pulses in the time domain. Fig. 1a shows the chirp matching in the frequency domain and Fig. 1b shows the same chirp-matching relationship in the time domain. In summary, based on the combination of PMs from type-I BiBO and type-I MgO:$LiNbO_3$ nonlinear crystals and optimization of the temporal overlapping of the pump and seed laser pulses in the DC-OPA process, an over-one-octave-bandwidth MIR laser pulse can be astoundingly realized. This method, which has the capability to amplify the over-one-octave bandwidth, called advanced DC-OPA, establishes a solid foundation for the experimental research.

In the designed sub-cycle, the chirp matching between the pump and seed laser pulses (Fig. 6a, black dashed line) effectively overlaps with the PM region of the BiBO crystal in the wavelength range of 1.2–2.4 μm. When the same chirp-matching relationship ($\Delta\lambda_{pump}/\Delta\lambda_{seed} \approx 0.038$) is applied to the PM regions of the two MgO:$LiNbO_3$ crystals, the overlapping areas can effectively support parametric amplification in the wavelength bands of 2.2–2.9 μm and 2.8–3.4 μm, respectively. Correspondingly, temporal overlapping between the seed laser pulse and three pump laser pulses is shown in Fig. 6b.

Nonlinear crystals

To further broaden the bandwidth of the seed laser, a 1-mm-thick BiBO crystal with a cutting angle of 60° for type-II PM in the x–z plane was employed in the DFG process for CEP-stable seed generation. The spectrum of the pump laser (0.8 μm) was broadened for the DFG process via optical filamentation in a 1.6 bar krypton gas cell[53], which was followed by a band-stop mirror for spectral reshaping[54] and a chirped mirror for dispersion compensation.

In the advanced DC-OPA module, a non-collinear geometric configuration was employed in both type-I BiBO and type-I MgO:$LiNbO_3$ crystals, with PM angles θ of 11.0° and 48.4°, respectively, and non-collinear angles α of 1.2° and 1.0°, respectively. In addition, the pre-amplifier and three subsequent amplifiers employed type-I MgO:$LiNbO_3$ crystals with dimensions of 10 × 10 × t6, 10 × 10 × t6, 10 × 10 × t5 and 20 × 20 × t4 mm^3, respectively. The three amplifiers also employed type-I BiBO crystals with dimensions of 10 × 10 × t5, 10 × 10 × t4 and 15 × 15 × t4 mm^3. Note that all the nonlinear crystals employed above are without an anti-reflection coating.

In the designed sub-cycle, high-energy MIR laser source, the non-collinear geometric configuration was adopted in a combination of one BiBO crystal and two MgO:$LiNbO_3$ crystals. The PM angles θ are 11.0°, 48.0° and 48.5°, which corresponded to non-collinear angles α of 0.6°, 0.5° and 2.1°, respectively.

Amplification chain based on the advanced DC-OPA scheme

We included some supporting functions to ensure the output quality of the MIR laser system. (1) As shown in Fig. 1b, the time delays of the pump and seed laser pulses were inconsistent for BiBO and MgO:$LiNbO_3$ crystals, so the time delay corresponding to each crystal needed to be independently adjusted. (2) To reduce the influence of the amplified parametric fluorescence, which particularly emerged under a high pump laser intensity, the pump laser pulses were separated to pump seven nonlinear crystals in total. (3) Because the beam profile of the amplified beam was strongly dependent on that of the pump beam, the image of the pump beam was relayed to the surface of each nonlinear crystal to maintain a flat-top-like profile for the pump beam. (4) We added intensity holes around the wavelengths of 1.8 and 2.5 μm to the seed laser spectrum via the AOPDF to avoid saturation around these wavelength regions. This greatly reduced the influence of spectral phase distortion caused by the reversed energy flow in the parametric process on the following compression work[46]. We also installed a nitrogen-filled sealed box to cover the advanced DC-OPA module to avoid adsorption by water in the air, which caused spectral phase distortion in the compression of high-energy IR/MIR laser pulses[47]. Supplementary Table 1 lists the parameters used in each amplification stage and the output performance of each amplifier.

Pulse duration

After the compression, we characterized the temporal profile of the compressed pulses using THG-FROG. Third-harmonic emission is produced from the input surface of a SiN plate irradiated by focusing the MIR beams using a parabolic mirror with a focal length of 50 mm.

CEP stability

Because the spectral bandwidth of the compressed MIR laser pulses was over one octave, the longer-wavelength components of the compressed pulses were frequency doubled by a $LiIO_3$ crystal and interfered with the shorter-wavelength components through a polarizer to generate the interference fringe. The time evolution of the f-to-2f interference fringes, which were in the wavelength region of 1.45–1.48 μm, is shown in Fig. 5a.

Beam profile

A 0.5 m focusing geometry was used to verify the focusability of the output MIR laser beam. In each measurement step, the diameters for the beam were calculated by fitting the measured profiles to a Gaussian function. The r.m.s. errors of the beam diameters in the fitting process are less than 0.03 on the x axis (horizontal direction) and 0.04 on the y axis (vertical direction), which provide sufficient accuracy for the measurements of beam diameters.

Data availability

Source data are provided with this paper. Additional raw data that support the findings of this study are available from the corresponding author upon reasonable request.

References

53. Hauri, C. P. et al. Generation of intense, carrier-envelope phase-locked few-cycle laser pulses through filamentation. *Appl. Phys. B* **79**, 673–677 (2004).

54. Ishii, N., Kaneshima, K., Kanai, T., Watanabe, S. & Itatani, J. Generation of ultrashort intense optical pulses at 1.6 μm from a bismuth triborate-based optical parametric chirped pulse amplifier with carrier-envelope phase stabilization. *J. Opt.* **17**, 094001 (2015).

Acknowledgements

We thank Y. Nabekawa for useful comments on measurement of the MIR pulse duration, B. Xue for support with THG-FROG and Y.-C Lin for discussion on the centre-of-gravity concept. We acknowledge financial support from the Ministry of Education, Culture, Sports, Science and Technology of Japan (MEXT) through Grants-in-Aid under grant no. 21H01850, and the MEXT Quantum Leap Flagship Program (Q-LEAP) (grant no. JP-MXS0118068681).

Author contributions

E.J.T. envisaged and initiated this research. Experimental studies and analysis were carried out by L.X., and guided and supervised by E.J.T. All authors discussed the results and contributed to the writing of the manuscript.

Competing interests

The authors declare no competing interests.

Additional information

Supplementary information The online version contains supplementary material available at https://doi.org/10.1038/s41566-023-01331-9.

Correspondence and requests for materials should be addressed to Eiji J. Takahashi.

Peer review information *Nature Photonics* thanks Giuseppe Sansone and the other, anonymous, reviewer(s) for their contribution to the peer review of this work.

Reprints and permissions information is available at www.nature.com/reprints.